<arttitle> Siberian flood basalt magmatism and Mongolia-Okhotsk slab dehydration

<aug> Alexei V. Ivanov[1] and Konstantin D. Litasov[2]

<aff> [1]Institute of the Earth's Crust, Siberian Branch, Russian Academy of Sciences, Lermontov street, 128, 664033 Irkutsk, Russia [2]Geophysical Laboratory, Carnegie Institution of Washington, 5251 Broad Branch Rd., NW, Washington DC 20015 USA.

<abs> Experimental data[1,2,3] combined with numerical calculations[4] suggest that fast subducting slabs are cold enough to carry into the deep mantle a significant portion of the water in antigorite, which transforms with increasing depth to phase A and then to phase E and/or wadsleyite by solid-solid phase transition. Clathrate hydrates and ice VII[4-6] are also stable at PT conditions of cold slabs and represent other potential phases for water transport into the deep mantle. Some cold slabs are expected to deflect while crossing the 410 km and stagnate in transition zone being unable to penetrate through 660 km discontinuity[7]. In this way slabs can move a long way beneath continents after long-lived subduction. With time, the stagnant slabs are heated to the temperature of the ambient transition zone and release free H_2O-bearing fluid[2]. Combining with transition zone water filter model[8] this may cause voluminous melting of overlying upper mantle rocks. If such process operates in nature, magmas geochemically similar to island-arc magmas are expected to appear in places relatively remote from active arcs at the time of their emplacement[9-10]. Dolerites of the south-eastern margin of the Siberian flood basalt province[11], located about 700 km from suggested trench, were probably associated with fast subduction of the Mongolia-Okhotsk slab[12-14] and originated by dehydration of the stagnant slab in the transition zone[11]. We show that influence of the subduction-related deep water cycle on Siberian flood basalt magmatism gradually reduced with increasing distance from the subduction zone.

<p> Cold subduction slabs can transport significant amount of water into the deep Earth. Major hydrated parts of the slab are oceanic sediments and underlying basaltic crust (e.g. ref. [15]). However, significant hydration (serpentinization) of the peridotite layer of the slab is also argued

(e.g. refs.[2,15]). Experimental studies of simplified and natural H_2O-bearing systems support the idea that significant amount of water can be transported to the deep Earth`s interior. Oceanic sediments (if being transported to the deep mantle) may contain high pressure topaz-OH and phase Egg, as well as clathrate hydrates and ice VII (see below) and basaltic crust can transport water as zoicite, lawsonite, and amphibole[15].

Fig. 1 summarizes the stability of hydrous minerals from experiments in the CaO-MgO-Al_2O_3-SiO_2-H_2O peridotite system at 800-1400 ^oC and 10-25 GPa[3]. At lower pressures, the boundaries are shown according to experiments in the Na_2O-CaO-FeO-MgO-Al_2O_3-SiO_2-H_2O peridotite[16]. The positions of phase boundaries are also extrapolated, using experimental data in MgO-SiO_2-H_2O and MgO-Al_2O_3-SiO_2-H_2O systems[17]. Besides, we show stability field (melting curve) of ice VII determined by Raman spectra in the externally heated diamond anvil cell (EHDC)[18]. Its position in PT space is in excellent agreement with the most recent experiment on ice VII melting curve obtained by both Raman spectra and X-ray diffraction in the EHDC[19]. Irrespective the experimental results on the melting of ice VII (see references for other experiments in[1,18-19]), it remains solid at the coldest slab PT path as suggested by Bina and Navrotsky[4] (Fig. 1). It has been shown (e.g. ref. [2]) that at the temperature slightly above the melting point of ice VII at a given pressure (along a curve similar to curve B in Fig. 1), antigorite undergoes a series of solid-solid transformations to other hydrous phases (which, with increasing pressure, are phase A, phase E, superhydrous phase B and phase D) without loss of its initial water content of about 3.7 wt. %. It is also well known that high-pressure modifications of olivine wadsleyite and ringwoodite can accommodate significant amount of water (up to 3 wt.% in their structures) (e.g. ref. [2-3]). The 10-Å[16] phase (the only phase, which contains molecular water among those discussed above) may be also important as a water carrier, especially in warmer subduction slabs at the conditions of so-called “choke point”, where severe dehydration melting related to island arc environments may take place. Another important source of subducting water, which might be previously underestimated are clathrate hydrates (gas hydrates)[5-6,20], which are stable in oceanic sediments, including accretionary prism sediments (e.g. ref[21]). They do not interact with surrounding sediments and can be accumulated in huge amounts. Subduction of clathrates is questionable, since they have low density relative to the host rocks, however, if their buoyancy force is not high, they can transport much water to the deep mantle. Fig. 1 shows that H_2-H_2O and Ar-H_2O clathrates are stable at PT path of

coldest type D slab. At higher pressure clathrates transform to corresponding ice (VI or VII depending on pressure). There are no experiments at high temperature with methane clathrate (common oceanic sediment gas hydrate), but it is expected to be stable at higher temperatures at corresponding pressures of from 0 to about 3 GPa compared to H_2-H_2O[22] (Fig. S1).

Summarising above statements, there are varieties of water-bearing mineral and crystalline hydrate to ice reactions, which allow the transport of water into the deep mantle by cold slabs (e.g. type D subduction, Fig. 1).

<p> Consider now a slab subducting rapidly along the PT path marked by a red dotted curve in Fig. 1, or at slightly higher temperatures. In dry conditions the temperature contrast between the slab and the ambient mantle will ensure that olivine is preserved while crossing the upper mantle – transition zone boundary at about 410 km depth[10]. An olivine-bearing slab in the wadsleyite-dominant transition zone will attain positive buoyancy and deflect to the horizontal[10]. If the slab can pass further through 410 km it will attain positive buoyancy at the transition zone – lower mantle boundary at about 660 km depth[10]. Olivine-wadsleyite transformation occurs at higher speed under the hydrous conditions[23]. Buoyancy of a dominantly dry slab with hydrated upper part was not modelled numerically. Irrespective the modelling it was well documented in seismic images worldwide that some slabs cannot sink deeper than transition zone (e.g. ref.[24]), but they move horizontally as long as subduction continues without break-off of the slab. (Alternatively, the slab can be fixed while the lithospheric plate runs over it. The effect remains the same; stagnant slab propagate beneath inner continental parts). This effect is known as slab stagnation. With time, the stagnant slab will heat up to the temperature of the ambient mantle along the horizontal part of the red dotted curve in Fig. 1. With increasing temperature phase E will decompose to wadsleyite and fluid, and then wadsleyite gradually lose its water to produce free H_2O-bearing fluid (Fig. 1). This fluid will arise to 410 km discontinuity, where it can be accumulated in dense hydrous melt[8] up to appropriate amount.

In the lowermost upper mantle water can be completely dissolved in the olivine structure if the total amount of H_2O does not exceed the water-capacity of the olivine at that depth (the preferred estimate of which is about 0.5 wt.% at 1200 ^{o}C and 12-14 GPa)[25-27]. The addition of 0.5 wt. % of water to the olivine structure has the same effect on olivine density as raising the

temperature by 240 ^{o}C[27]. Thus, release of water from the stagnant slab is equivalent to heating the mantle above by a value considered sufficient for a thermally buoyant mantle plume (e.g., ref[28]). A water-driven mantle diapir (a plume in the fluid dynamical sense) will rise by its own buoyancy and melt on crossing its wet solidus beneath thick cratonic lithosphere (Fig. 1). Such a water cycle, linked to cold subduction, slab stagnation and wet diapir rising, is expected to result in magmatism similar to that seen in island arc systems, but at larger distance from a trench and induced by slab dehydration at greater depths[2,9-11].

<p> The effect of water on trace elements in subduction systems is well understood; water carries from dehydrating slabs large ion lithophile elements such as Ba, K and Sr and light rare earth elements such as La, but it is not able to carry high field strength elements such as Ti and Nb[29]. It also fractionates Th and U[29]. High degree partial melting of the water-saturated source above subducting slabs yields magmas with typical island arc basalt trace element patterns with low high-field-strength- and high large-ion-lithophile-element abundances and depletion of Th relative to U.

<p> The Siberian Traps flood basalt province with its dominant low-Ti basalt type and 'subduction' trace-element fingerprints[30] lay in a back-arc of the Mongolia-Okhotsk subduction at the time of flood basalt eruption[10,12-14,31] (Fig. 2). Thus it is a good candidate to test the subduction-related transition zone water-cycle model[2,9-11] and its influence on postulated lower mantle plume-related flood basalt magmatism[28].

<p> Subduction from south (in present-day coordinates) beneath Siberia is documented from the Devonian until the closure of the Mongolia-Okhotsk Ocean in the Late Jurassic[13] or Early Cretaceous[14]. Siberian Trap magmatism lasted as long as 22-26 Ma from the Late Permian until the Middle Triassic as shown by U-Pb and ^{40}Ar/^{39}Ar geochronologic data (see review[10]). Overall long duration is independently supported by paleomagnetic data[32]. Paleotectonic reconstruction of subduction beneath the Siberian part of Pangea at Permo-Triassic time[12], which is the time of the major pulse of the Siberian Traps flood basalt emplacement[33], is shown in Fig. 2. Similar paleotectonic reconstructions can be found elsewhere[10,13-14,31]. Remnants of the Mongolia-Okhotsk slab are still recognizable in seismic tomography images beneath Siberia[14].

<p> Fig. 3 shows trace-element patterns of Early to Middle Triassic (see Supplementary Information) dolerite sills in the Angara-Taseevskaya syncline, which belongs to the south-eastern (in present-day coordinates) Siberian Traps flood basalt province. The original data[11] for rocks are recalculated back to their initial melt compositions according to the procedure described in Methods and Supplementary Information. The original and recalculated values are listed in Table S1. The initial melt compositions of the south-eastern Siberian Trap flood basalt province are remarkably similar to the initial melt compositions of the modern arc of Eastern Kamchatka[34] suggesting a similar model for their origin in relation with dehydration of subducting slabs. Fig. 4 shows a profile of Nb/La ratio in basaltic rocks from the rifted active continental margin of the Siberia (Transbaikalian belt[35]) through the Siberian flood basalt province (the Angara-Taseevskaya syncline[11], Tunguska syncline[36] and Noril'sk[37]). The Nb/La ratio gradually increases from the typically low island-arc values[34] in proximity to the Mongolia-Okhotsk subduction system towards typically high ocean island basalt values[38] at Noril'sk, showing the decreasing influence of subduction on the trace element budget of the flood basalts.

<p> The size and volume of the Siberian flood basalt province is enormous. The size is almost the same as the present-day Australian continent and the most reliable estimations of the volume are close to 4×10^6 km^3; neither can easily be explained by any model, and this includes the plume model in its classic form[28] (see review[10]). Incorporation of water in the source of melting significantly lowers the solidus compared to the dry mantle (Fig. 1) and allows voluminous melting with reasonable temperature anomalies. Subduction of the Mongolia-Okhotsk slab probably played a dominant role in the origin of the Siberian flood basalt province. Probably a combination of a temperature anomaly[28], recycling of fusible eclogite to sublithospheric depth[39] and a hydrated source[10-11] could explain the extremely voluminous melting of the Siberian Traps and its enormous size. Relatively short duration of Siberian Traps volcanism[10,32-33] compared to continuous arc-type volcanism and episodic nature of flood basalt volcanism[10] are probably due to rare events of ultrahigh speed subduction (up to 20 cm/yr) (type D in Fig. 1) and uneven distribution of gas hydrates in accretionary prisms[21].

<meth1ttl> 'Methods'.

<meth1hd> To calculate the initial melt compositions of the Angara-Taseevskaya sills, Mg-number ($Mg/(Mg+0.85Fe_{total}$) and Sr/Pr ratios were used as proxies of crystal fractionation of olivine and plagioclase, respectively (see Fig. S2). The role of clinopyroxene and rutile fractionation was estimated through CaO/Al_2O_3 and Th/U variations to be not important compared to olivine and plagioclase[11]. A model of equilibrium fractionation was applied[40] for recalculating all elements plotted in Fig. 3. Bulk distribution coefficients were calculated from olivine/melt and plagioclase/melt distribution coefficients listed in Table S2. Proportions of these minerals were estimated from Mg-number versus Sr/Pr diagram (Fig. S2). After addition of olivine and plagioclase the Mg-number in recalculated compositions became close to 0.7, the usual value used to testify equilibrium with mantle peridotite. Comparison between measured and recalculated values is shown in Fig. S3. Both datasets reveal similarities with the island arc basalts, but the similarity is enhanced in the recalculated dataset, mainly due to the effect of the plagioclase fractionation on Sr.

<bibcit> 1. Lin J.F., Schwegler E. & Yoo C.-S. in *Earth's deep water cycle, Geophysical monograph 168* (eds Jacobsen, S.D. & Van der Lee, S.) 159-170 (American Geophysical Union, Washington DC 2006).

<bibcit> 2. Komabayashi, T. in *Earth's deep water cycle, Geophysical monograph 168* (eds Jacobsen, S.D. & Van der Lee, S.) 29-43 (American Geophysical Union, Washington DC 2006).

<bibcit> 3. Litasov, K. & Ohtani, E. Stability of various hydrous phases in CMAS pyrolite-H_2O system up to 25 GPa. *Phys. Chem. Minerals* **30,** 147-156 (2003).

<bibcit> 4. Bina, C.R. & Navrotsky A. Possible presence of high-pressure ice in cold subducting slabs. *Nature* **408**, 844-847 (2000).

<bibcit>5. Vos, W.L., Finger, L.W., Hemley R.J. & Mao, H.-K. Novel H_2-H_2O clathrates at high pressures. *Phys. Rev. Lett.* **71**, 3150-3153 (1993).

<bibcit> 6. Manakov, A.Yu., Voronin, V.I., Kurnosov, A.V., Teplykh, A.E., Komarov, V.Yu. & Dyadin, Yu.A. Structural investigations of argon hydrates at pressures up to 10 kbar. *J. Inclusion Phenomena Macrocyclic Chem.* **48**, 11-18 (2004).

<bibcit> 7. Bina, C.R., Stein, S., Marton, F.C. & Van Ark, E.M. Implications for slab mineralogy for subduction dynamics. *Phys. Earth Planet. Int.* **127,** 51-66 (2001).

<bibcit> 8. Bercovici, D., & Karato, S.-I., Whole-mantle convection and the transition-zone water filter. *Nature* **425**, 39-44 (2003).

<bibcit> 9. Ivanov, A.V. & Balyshev, S.V. in *Plates, plumes and paradigms, Geological Society of America Special Paper 388* (eds Foulger, G.R., Natland, J.H., Presnall, D.C. & Anderson, D.L.) 327-346 (Geological Society of America, Princeton 2005).

<bibcit> 10. Ivanov, A.V. in *The origin of melting anomalies: Plates, plumes and planetary processes, Geological Society of America Special Paper* 430 (eds Foulger, G.R. & Jurdy, D.M.) 635-668 (Geological Society of America, Princeton 2007).

<bibcit> 11. Ivanov, A.V., Demonterova, E.I., Rasskazov, S.V. & Yasnygina, T.A. Low-Ti melts from the Southeastern Siberian Traps Large Igneous Province: Evidence for a water-rich mantle source? *J. Earth System Sci., in press*

<bibcit> 12. Enkin, R.J., Yang, Z., Chen, Y. & Courtillot, V. Paleomagnetic constraints on the geodynamic history of major blocks of China from the Permian to the Present. *J. Geophys. Res.* **97**, 13953–13989 (1992).

<bibcit> 13. Zorin, Y.A. Geodynamics of the western part of the Mongolia-Okhotsk collisional belt, Trans-Baikal region (Russia) and Mongolia. *Tectonophysics* **306,** 33-56 (1999).

<bibcit> 14. Van der Voo, R., Spakman, W. & Bijwaard, H. Mesozoic subducted slabs under Siberia. *Nature* **397**, 246-249 (1999).

<bibcit> 15. Arcay, D., Doin, M.-P., Tric, E. & Bousquet, R. Influence of postcollisional stage on subduction dynamics and the buried crust thermal state: insights from numerical simulations. *Tectonophysics* **441**, 27-45 (2007).

<bibcit> 16. Fumagalli, P. & Poli, S. Experimentally determined phase relations in hydrous peridotites to 6.5 GPa and their consequences on the dynamics of subduction zones. *J. Petrol.* **46**, 555-578 (2005).

<bibcit> 17. Komabayashi, T., Hirose, K., Funakoshi, K.-I. & Takafuji, N. Stability of phase A in antigorite (serpentine) composition determined by in-situ X-ray pressure observations. *Phys. Earth Planet. Inter.* **151**, 276-289 (2005).

<bibcit> 18. Lin, J. F., Militzer, B., Struzhkin, V.V., Gregoryanz, E., Hemley, R.J. & Mao, H.-K. High pressure-temperature Raman measurements of H_2O melting to 22 GPa and 900 K. *J. Chem. Phys.* **121**, 8423–8427 (2004).

<bibcit> 19. Dubrovinsky, L. & Dubrovinskaia, N. in *Advances in high-pressure mineralogy, Geological Society of America Special Paper* 421 (ed Ohtani, E.) 105-114 (Geological Society of America, Princeton 2007).

<bibcit> 20. Hirai, H., Uchihara, I., Fujihisa, H., Sakashita, M., Katoh, E., Aoki, K., Yamamoto, Y., Nagashima, K.& Yagi, T. High-pressure structures of methane hydrate. J. Phys.: Condens. Matter 14, 11443-11446 (2002).

<bibcit> 21. Saito, H. & Suzuki, N. Terrestrial organic matter controlling gas hydrate formation in the Nankai Trough accretionary prism, offshore Shikoku, Japan. *J. Geochem. Exploration* **95**, 88-100 (2007).

<bibcit> 22. Skiba, S.S., Larionov, E.G., Manakov, A.Y., Kolesov, B.A. & Kosyakov, V.I. Investigation of hydrate formation in the system H_2-CH_4-H_2O at a pressure up to 250 MPa. *J. Phys. Chem. B.* **111**, 11214-11220 (2007).

<bibcit> 23. Hosoya, T., Kubo, T., Ohtani, E., Sano, A. & Funakoshi, K.-I. Water controls the fields of metastable olivine in cold subducting slabs. *Geophys. Res. Lett.* **32**, L17305 (2005).

<bibcit> 24. Fukao, Y., Widiyantoro, S. & Obayashi, M. Stagnant slabs in the upper and lower mantle transition region. *Rev. Geophys.* **39**, 291-323 (2001).

<bibcit> 25. Hirschmann, M.M., Aubaud, C. & Withers, A.C. Storage capacity of H_2O in nominally anhydrous minerals in the upper mantle. *Earth Planet. Sci. Lett.* **236,** 167-181 (2005).

<bibcit> 26. Litasov, K.D., Ohtani, E., Kagi, H., Jacobsen, S.B., & Ghosh, S. Temperature dependence and mechanism of hydrogen incorporation in olivine at 12.5-14.0 GPa. *Geophys. Res. Lett*. **34**, L16314, doi:10.1029/2007GL030737 (2007).

<bibcit> 27. Smyth, J.R., Frost, D.J., Nestola, F., Holl, C.M. & Bromiley, G. Olivine hydration in the deep upper mantle: Effect of temperature and silica activity. *Geophys. Res. Lett.* **33,** 953 L15301 (2006).

<bibcit> 28. Campbell, I.H. & Griffiths, R.W. Implications of mantle plume structure for the evolution of flood basalts. *Earth Planet. Sci. Lett.* **99**, 79–93 (1990).

<bibcit> 29. McCulloch, M.T. & Gamble, J.A. Geochemical and geodynamical constraints on subduction zone magmatism. *Earth Planet. Sci. Lett.* **102**, 358–374 (1991).

<bibcit> 30. Puffer, J.H. Contrasting high filed strength element content of continental flood basalts from plume versus reactivated-arc sources. *Geology* **29,** 675-678 (2001).

<bibcit> 31. Nikishin, A.M., Ziegler, P.A., Abbott, D., Brunet, M.-F. & Cloetingh, S. Permo-Triassic intraplate magmatism and rifting in Eurasia: implications for mantle plumes and mantle dynamics. *Tectonophysics* **351,** 3-39 (2002).

<bibcit> 32. Steiner, M.B. in *Non-Marine Permian Biostratigraphy and Biochronology, Geological Society Special Publications 265* (eds Lucas, S.G., Cassinis, G., Schneider, G. & Schneider, J.W.) 15-38 (London 2006).

<bibcit> 33. Renne, P.R. & Basu, A.R. Rapid eruption of the Siberian Traps flood basalts at the Permo-Triassic boundary; *Science* **253,** 176-179 (1991).

<bibcit> 34. Portnyagin, M., Hoernle, K., Plechov, P., Mironov, N. & Khubunaya, S. Constraints on mantle melting and composition and nature of slab components in volcanic arcs from volatiles (H_2O, S, Cl, F) and trace elements in melt inclusions from the Kamchatka Arc. *Earth Planet. Sci. Lett.* **255,** 53-69 (2007).

<bibcit> 35. Yarmolyuk, V.V., Litvinovsky, B.A., Kovalenko, V.I., Jahn, B.M., Zanvilevich, A.N., Vorontsov, A.A., Zhuravlev, D.Z., Posokhov, V.F., Kuz'min, D.V. & Sandimirova, G.P. Formation stages and sources of the peralkaline granitoid magmatism of the Northern Mongolia-Transbaikalia rift belt during the Permian and Triassic. *Petrology* **9,** 302-328 (2001).

<bibcit> 36. Al'mukhamedov, A.I., Medvedev, A.Ya. & Zolotukhin, V.V. Chemical Evolution of the Permian-Triassic Basalts of the Siberian Platform in Space and Time. *Petrology* **12,** 297-311 (2004).

<bibcit> 37. Wooden, J.L., Czamanske, G.K., Fedorenko, V.A., Arndt, N.T., Chauvel, C., Bouse, R.M., King, B.-S.W., Knight, R.J. & Siems, D.F. Isotopic and trace-element constraints on mantle

and crustal contributions to characterization of Siberian continental flood basalts, Noril'sk area, Siberia. *Geochim. Cosmochim. Acta* **57,** 3677-3704 (1993).

<bibcit> 38. Sun, S.S. & McDonough, W.F. in *Magmatism in the oceanic basins, Geological Society Special Publication 42* (eds Sounders, A.D. & Norry, M.J.) 313-345 (Geological Society London, London 1989).

<bibcit> 39. Sobolev, A.V., Hofmann, A.W., Kuzmin, D.V., Yaxley, G.M., Arndt, N.T., Chung, S.-L., Danyushevsky, L.V., Elliot, T., Frey, F.A., Garcia, M.O., Gurenko, A.A., Kamenetsky, V.S., Kerr, A.C., Krivolutskaya, N.A., Matvienkov, V.V., Nikogosian, I.K., Rocholl, A., Sigurdsson, I.A., Sushchevskaya, N.M. & Teklay, M. The amount of recycled crust in sources of mantle-derived melts. *Science* **316,** 412-417 (2007).

<bibcit> 40. Shaw, D.M. Trace element fractionation during anatexis. *Geochim. Cosmochim. Acta.* **34,** 237-243 (1970).

<bibcit> 41. Turcotte, D.L. & Schubert, G. *Geodynamics* (Cambridge University Press, Cambridge, ed. 2, 2002).

<bibcit> 42. Hirschmann, M.M. Mantle solidus. Experimental constraints and the effect of peridotite composition. *Geochem. Geophys. Geosyst.* **24**, 2000GC000070 (2000).

<supp> '**Supplementary Information** accompanies the paper on **www.nature.com/nature**.'

<ack> The m/s was initiated by two consequent presentations given by A.V.I. at Paleomagnetism and Geochronology Lab of Institute of Geology and Geophysics of Chinese Academy of Sciences (Beijing, China) and at Geological unit of Institute of the Earth's Crust of Siberian Branch of the Russian Academy of Sciences (Irkutsk, Russia). It benefited from questions and discussions during and after the presentations. Gillian Foulger is particularly thanked for useful recommendations on reworking of the text.

<corr> Correspondence and requests for materials should be addressed to aivanov@crust.irk.ru.

<LEGEND> Figure 1. Stability of water-bearing minerals and ice VII at mantle conditions[1,2,3,16-18]. The pressure is shown only to 20 GPa (~600 km depth) and temperature is limited to 1700 ^{o}C for the sake of simplicity. Solid curve marked M is for typical mantle geotherm[41]. Other solid curves

are for coldest parts of four types of subducting slabs, referred to as A, B, C and D[4]. Positions of wet (2 wt.% of H_2O)[3] and dry[42] solidus of peridotite type mantle are shown by dotted black curves. Coldest type D represents a fast subduction up to ~20 cm/yr[4]. Decreasing degree of saturation of blue colour represents relative decrease of water in the water-bearing assemblages[3] (Chl – chlorite, Amph – amphibole, 10Å – 10-Å phase, Atg – antigorite, phA – phase A, SuB – superhydrous phase B, Wd – wadsleyite, Rw – ringwoodite, Cpx – clinopyroxene). Stability field of ice VII is superimposed on stability fields of other minerals. Yellow star marks invariant point of ice II-like and diamond-like H_2-H_2O clathrate structures with corresponding fluid phases[5]. Yellow and green lines show melting curve of the H_2-H_2O and Ar-xH_2O clathrates, respectively[5-6]. General feature of experimental studies with clathrate hydrates is that clathrates are stable at higher temperatures than corresponding pure high pressure H_2O ices. Methane hydrate is stable at higher temperatures than H_2-H_2O clathrate at given pressure (for example, about 40 ^oC difference was experimentally observed at 250 MPa[22], see also Fig. S1). Red dotted curve with numbers in white circles shows PT path of water recycling within cold subducting slab (1), within stagnant slab (2) and within rising water-rich mantle diapir (3). Crossing the wet solidus at about 300 km depth the rising diapir starts to melt (4). The melt erupted on the surface (5) should have the geochemical fingerprints of island arc basalts (see text).

<LEGEND> Figure 2. Paleotectonic reconstructions of the Mongolia-Okhotsk Ocean and its surroundings at Permo-Triassic time[12]. For the sake of simplicity all different terranes indicated by names are shown in the same light brown colour without boundaries between them. The coeval Siberian Traps flood basalt province is shown in green. Black arrow indicates present-day north. White stars indicate localities discussed in the text: TB – Transbaikalian rifted margin[35], ATS – Angara-Taseevskaya syncline[11], TS – Tunguska syncline[36], N – Noril'sk[37].

<LEGEND> Figure 3. Primitive mantle[38] normalized diagram for initial melts of the Angara-Taseevskaya syncline (bold lines). Original measured compositions[11] were recalculated (corrected) to the initial melt compositions by adding olivine and plagioclase (see Methods). Shadowed field represent compositional range of the initial melts of the modern arc of Eastern Kamchatka[34]. The modelled primary basaltic melt composition of ocean islands (OIB[38]) is drastically different from those of the Angara-Taseevskaya syncline. Slight difference in trace element abundances of the

Angara-Taseevskaya and Kamchatka primary melts may be due to the difference in depth of their respective slab dehydrations (and thus difference in partitioning of elements into water fluid), difference in depth of melting (shallower beneath Kamchatka and deeper beneath Siberia) and approximations in the correction procedure (see Supplementary Material).

<LEGEND> Figure 4. Nb/La variations in basaltic rocks from the rifted margin of Siberia through the Siberian flood basalt province. MOSZ – Mongolia-Okhotsk suture zone, which represents the boundary between the Siberian and Mongolian terranes[12] and can be considered as the approximate position of the trench at the time of subduction of the Mongolia-Okhotsk slab. Original Nb/La ratios[11,35-37] (not recalculated to crystal fractionation) are plotted. This ratio was chosen because it is least affected by olivine and plagioclase fractionation (Fig. S4) compared to other key trace-element ratios for defining subduction setting versus within-plate setting (e.g. K/Nb, Sr/Pr, Ce/Pb). Small black squares are for individual samples. Large white circles are for average compositions. For the Tunguska syncline only the average compositions of three large lava units were published[36]. IAB – island arc basalts[34]. OIB – ocean island basalts[38]. Other acronyms as in Fig. 3. Black triangles are for subset of samples from upper Gudchikhinsky sub-suite of Noril'sk for which 100% olivine-free pyroxenite was suggested as a source; the source created after melting of a plume-recycled-eclogite and reaction of the eclogite-derived melt with peridotitic mantle[39]. Large white square is for average composition of the upper Gudchikhinsky sub-suite. Involvement of recycled eclogite tends to increase Nb/La ratio and thus can not explain subduction fingerprints. Suggested lower crustal contamination[37] can not fully explain trace element variations either, because significant part of volcanic units in Noril'sk and other regions of the Siberian Traps with non-DUPAL isotopic signatures (e.g. $\Delta 8/4Pb < 50$, $^{87}Sr/^{86}Sr < 0.705$) belong to low-Ti rock type with subduction fingerprints[10-11].

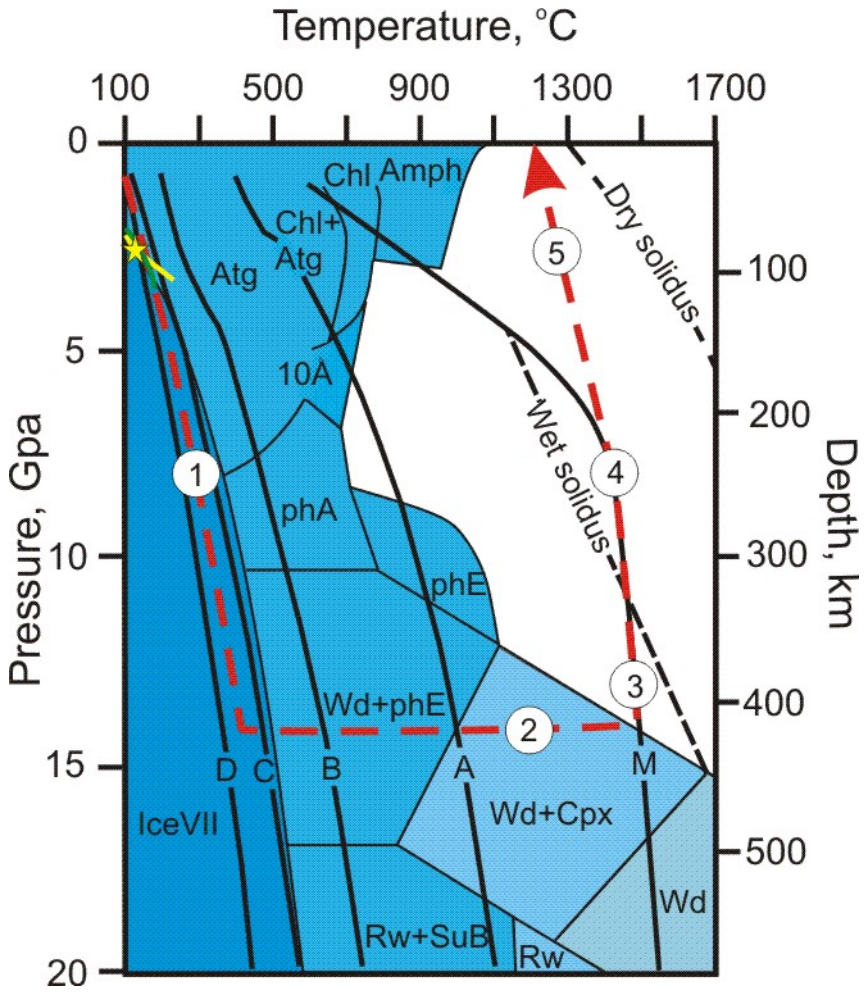

Figure 1.

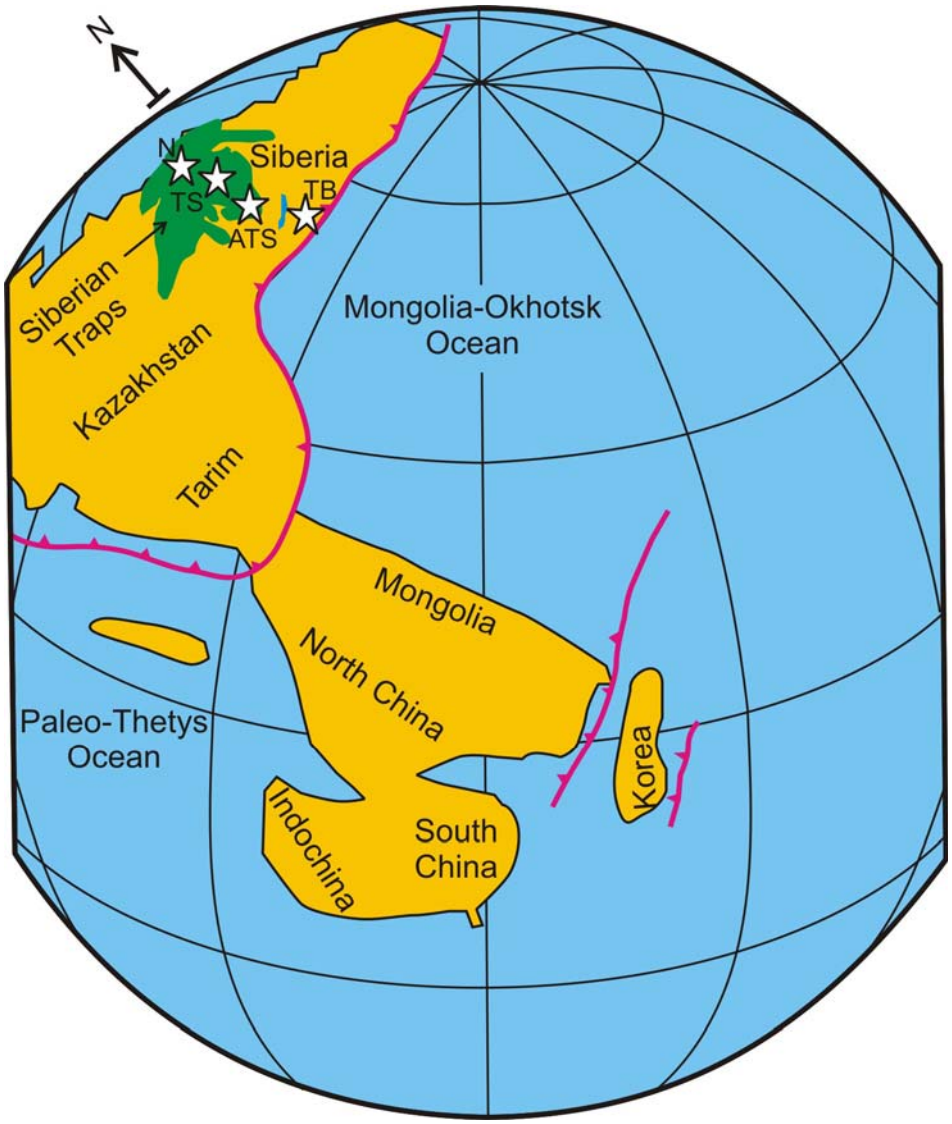

Figure 2.

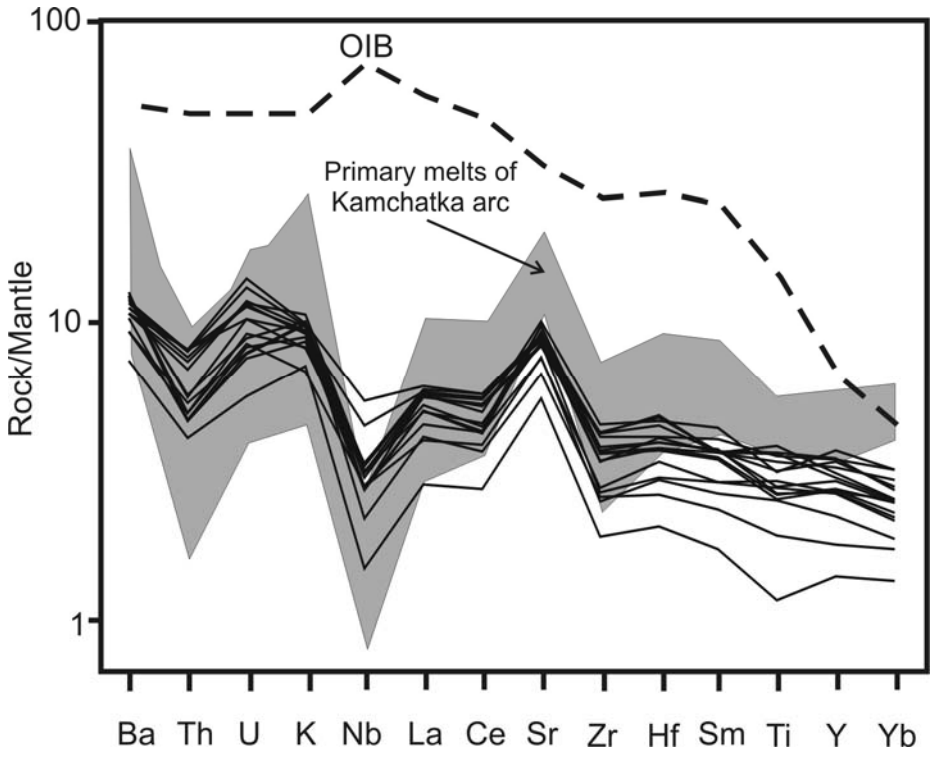

Figure 3.

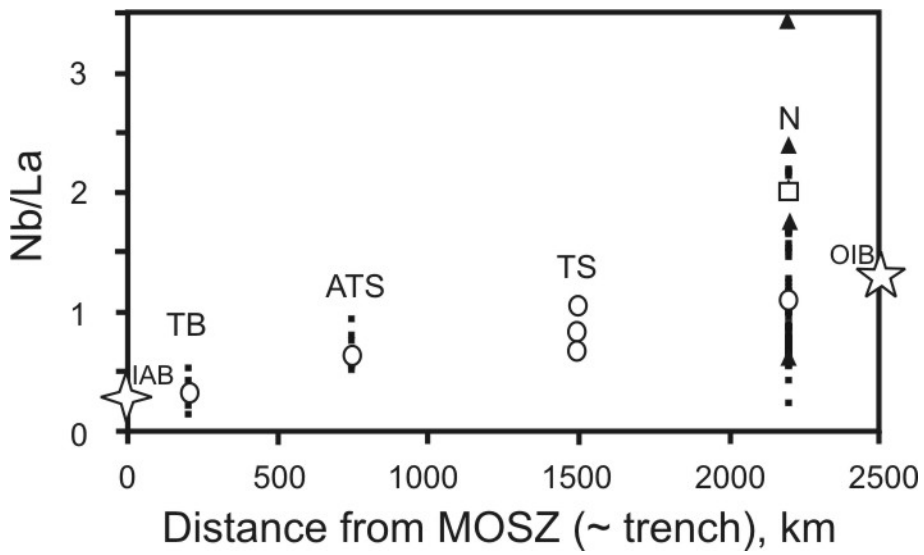

Figure 4.

Supplementary Information for paper "Siberian flood basalt magmatism and Mongolia-Okhotsk slab dehydration"

Fig. S1 is a summary of experiments[1-3] with clathrate hydrates, which show that methane hydrate (common oceanic gas hydrate) is stable at higher temperature compared to hydrogen and argon hydrates.

Dolerite sills in the Angara-Taseevskaya syncline were considered to be an intrusive formation of the Siberian Traps as early as 1873 by Alexander Czekanowski[4]. Similar dolerite intrusions are abundant throughout the entire Siberian Traps province exposed in the Siberian craton. In total, the volume of intrusions was estimated to be as large as 0.8×10^6 km^3, which is nearly a half of the preserved volume of lava and volcanoclastic deposits[5] (also see[6] for review). The geology and petrography of the sills within the Angara-Taseevskaya syncline were studied in detail in the 1960-1970s[7-8]. The sills were recently dated using the $^{40}Ar/^{39}Ar$ technique to be Early to Middle Triassic[9-10]. Study of major and trace elements has shown that compositional variations of the sills are controlled by olivine and plagioclase fractionation[11] in general agreement with earlier petrographic records[7-8]. The concentrations of selected elements for the dolerites of the sills are listed in Table S1.

<p> Mg-number ($Mg/(Mg+0.85Fe_{total}$) and Sr/Pr ratios were used as proxies for crystal fractionation of olivine and plagioclase, respectively (see Fig. S2). To fit observed variations in Fig. S2 the model of equilibrium crystallization[12] of plagioclase and olivine was used. $D^{Mg/Fe}$ of 2.8 for olivine was used to model Mg-number variations. Mineral/melt distribution coefficients for Sr and Pr to model plagioclase fractionation are listed in Table S2. Proportions of fractionated olivine and plagioclase derived from the Fig. S2 were taken to calculate bulk distribution coefficients from mineral/melt distribution coefficients (Table S2) to recalculate all measured concentrations in rocks to their initial melts with the amount of added olivine and plagioclase derived from the Fig. S2. Originally measured concentrations and those in the calculated initial melts are provided in Table S1. Fig. S3A compares these two datasets. Initial melts are lower in abundance of all trace elements due to the bulk distribution coefficients for all elements below 1. The general patterns in the both datasets are similar with the exception of Sr, because Sr is compatible ($D > 1$) in plagioclase[14] (Table S2). Fractionated rocks (those with low Mg-number) are characterized by Sr depletion relative to neighboring elements, whereas their initial melts are characterized by Sr enrichment. The recalculation procedure was not robust and could lead to overcorrection. To show that this potential problem does not invalidate the conclusion, the compositions of initial melts of the three most magnesium-reach (least fractionated) samples are plotted in Fig.3B together with the range of initial melts for the East Kamchatka arc[13]. It may be seen that the initial melts of the least fractionated sills of the Angara-Taseevskaya syncline and those of the typical island arc tectonic setting are indeed remarkably similar to each other.

<p> Nb/La ratio can be used as a proxy of subduction influence because it is not affected by crystal fractionation of plagioclase and olivine (Fig. S4). Nb/La is about 0.3 and 1.3 in modeled ocean island basalts[15] and parental melts of Kamchatka arc[13], respectively.

<bibcit> 1. Vos, W.L., Finger, L.W., Hemley R.J. & Mao, H.-K. Novel H_2-H_2O clathrates at high pressures. *Phys. Rev. Lett.* **71**, 3150-3153 (1993).

<bibcit> 2. Manakov, A.Yu., Voronin, V.I., Kurnosov, A.V., Teplykh, A.E., Komarov, V.Yu. & Dyadin, Yu.A. Structural investigations of argon hydrates at pressures up to 10 kbar. *J. Inclusion Phenomena Macrocyclic Chem.* **48**, 11-18 (2004).

<bibcit> 3. Skiba, S.S., Larionov, E.G., Manakov, A.Y., Kolesov, B.A. & Kosyakov, V.I. Investigation of hydrate formation in the system H2-CH4-H2O at a pressure up to 250 MPa. *J. Phys. Chem. B.* **111**, 11214-11220 (2007).

<bibcit> 4. Masaitis, V.L. In: *A.L. Czekanowski. Collection of unpublished manuscripts of A.L. Czekanowski and papers about his scientific work,* (ed Obruchev, S.V.) 41-46 (Irkutsk book publisher, Irkutsk 1962) (In Russian).

<bibcit> 5. Vasil'ev, Yu.R., Zolotukhin, V.V., Feoktistov, G.D. & Prusskaya, S.N. Evaluation of the volumes and genesis of Permo-Triassic Trap magmatism of the Siberian Platform. *Geologiya i Geofizika* **41**, 1696-1705 (2000) (In Russian).

<bibcit> 6. Ivanov, A.V. in *The origin of melting anomalies: Plates, plumes and planetary processes, Geological Society of America Special Paper* 430 (eds Foulger, G.R. & Jurdy, D.M.) 635-668 (Geological Society of America, Princeton 2007).

<bibcit> 7. Feoktistov, G.D., *Petrography of traps from water-drain area of the middle current of the Angara river.* (Transactions of East-Siberian Geological Institute, issue 7, Irkutsk 1961) (In Russian).

<bibcit> 8. Feoktistov, G.D., *Petrology and conditions for formation of trap sills.* (Nauka, Novosibirsk 1978) (In Russian).

<bibcit> 9. Ivanov, A.V., Rasskazov, S.V., Feoktistov, G.D., He, H., Boven, A. $^{40}Ar/^{39}Ar$ dating of Usol'skii sill in the southeastern Siberian Traps Large Igneous Province: evidence for long-lived magmatism. *Terra Nova* **17**, 203-208 (2005).

<bibcit> 10. Ivanov, A.V., He, H., Liekun, Y., Nikolaeva, I.N. & Palesskii, S.V. $^{40}Ar/^{39}Ar$ dating of intrusive magmatism in the Angara-Taseevskaya syncline and its implication for duration of magmatism of the Siberian Traps. *J. Asian Earth Sci. submitted.*

<bibcit> 11. Ivanov, A.V., Demonterova, E.I., Rasskazov, S.V. & Yasnygina, T.A. Low-Ti melts from the Southeastern Siberian Traps Large Igneous Province: Evidence for a water-rich mantle source? *J. Earth System Sci., in press*

<bibcit> 12. Shaw, D.M. Trace element fractionation during anatexis. *Geochim. Cosmochim. Acta.* **34,** 237-243 (1970).

<bibcit> 13. Portnyagin, M., Hoernle, K., Plechov, P., Mironov, N. & Khubunaya, S. Constraints on mantle melting and composition and nature of slab components in volcanic arcs from volatiles (H_2O, S, Cl, F) and trace elements in melt inclusions from the Kamchatka Arc. *Earth Planet. Sci. Lett.* **255,** 53-69 (2007).

<bibcit> 14. Dun, T. & Sen, C. Mineral/matrix partition coefficients for orthopyroxene, plagioclase, and olivine in basaltic to andesitic systems: A combined analytical and experimental study; *Geochim. Cosmochim. Acta.* **58** 717-733. 1994

<bibcit> 15. Sun, S.S. & McDonough, W.F. in *Magmatism in the oceanic basins, Geological Society Special Publication 42* (eds Sounders, A.D. & Norry, M.J.) 313-345 (Geological Society London, London 1989).

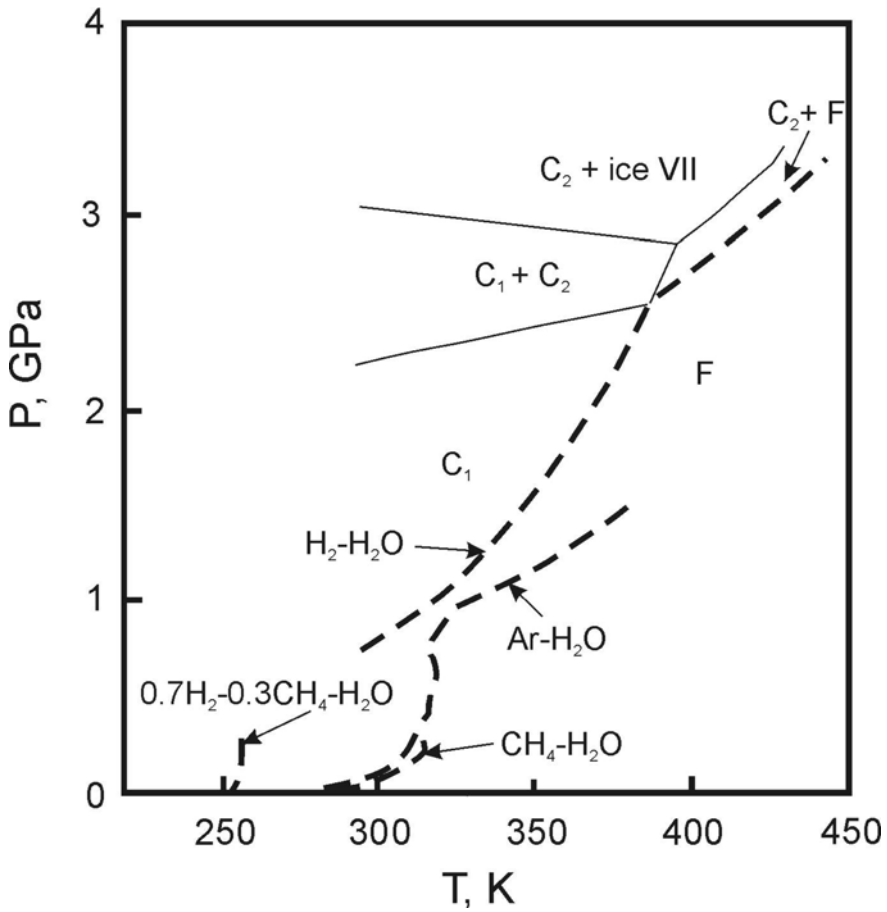

Figure S1. Comparison of melting curves of hydrogen-, argon- and methane hydrates[1-3], shown as corresponding bold dashed lines. F is for fluid. C_1 and C_2 are high-pressure crystalline structures of hydrogen hydrate.

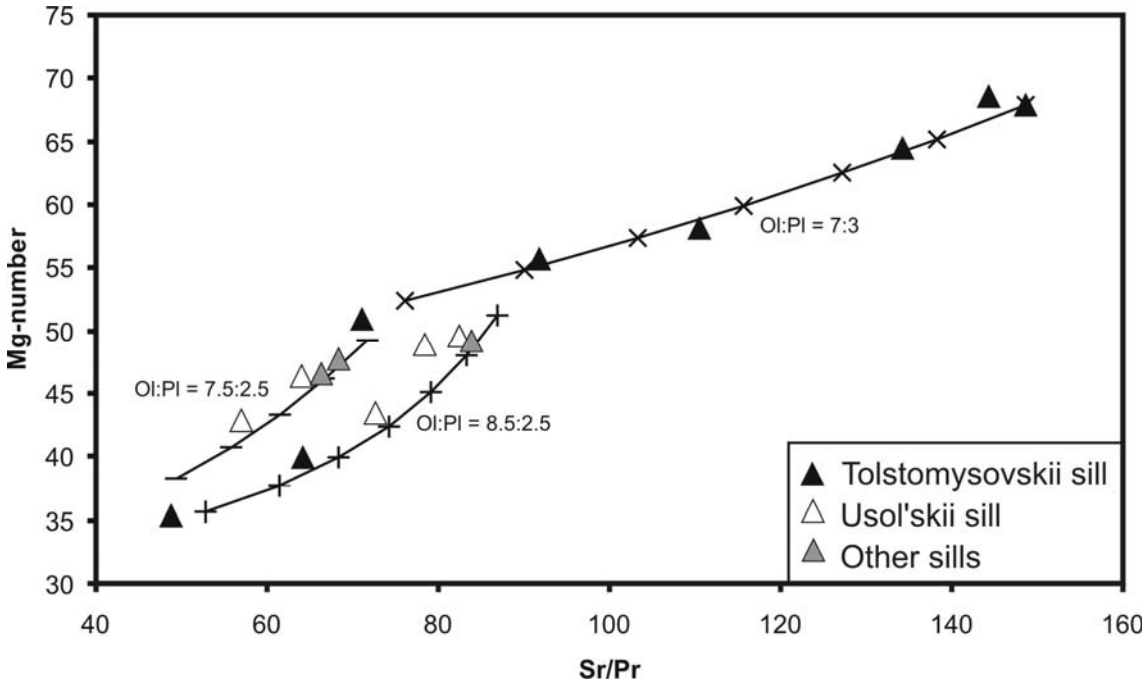

Figure S2. Mg-number versus Sr/Pr in dolerites from sills from the Angara-Taseevskaya syncline. Original data from[10-11] (see also Table S1). Curves with ticks represent modeled curves of olivine (Ol) and plagioclase (Pl) equilibrium fractionation. Each tick is for 0.1 fraction of olivine and plagioclase. Proportions of the fractionated minerals are shown in the Figure.

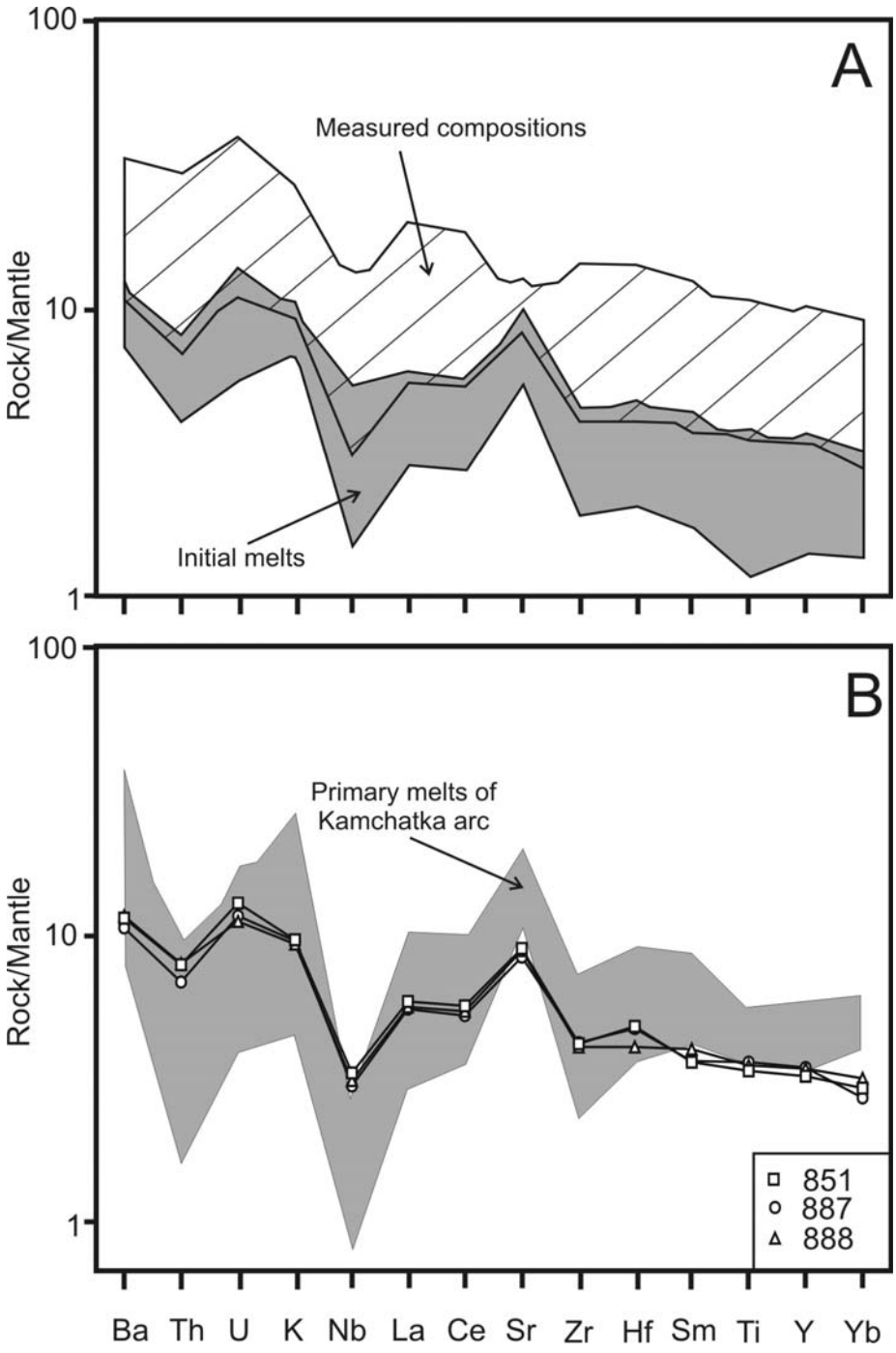

Figure S3. Comparison of measured and recalculated (initial melt) compositions of the Angara-Taseevskaya dolerites (Figure A) and comparison of the initial melts of high Mg-number dolerites (least fractionated and thus least corrected) with initial melts of the modern arc of Eastern Kamchatka[13] (Figure B). Data are from Table S1.

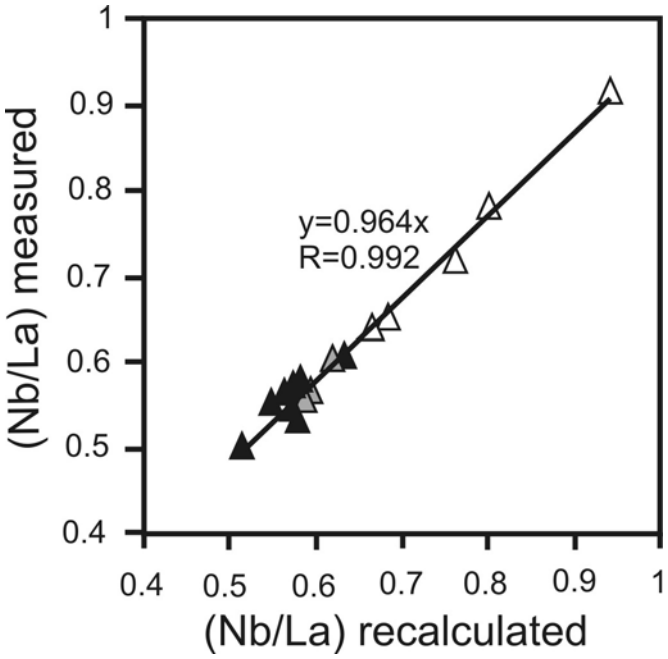

Figure S4. Comparison of measured and recalculated Nb/La in the Angara-Taseevskaya dolerites. Symbols as in Fig. S2. Linear regression forced trough zero is shown as bold line.

Table S1. Selected major and trace elements for Angara-Taseevskaya dolerites[10-11] and their initial melts[this study]. Mg# - Mg-number. Concentrations of all trace elements are in ppm and those of TiO_2 and K_2O are in wt. %.

Sill	Tolstomysovskii							
Sample	833		834		847		851	
	Meas.	Initial	Meas.	Initial	Meas.	Initial	Meas.	Initial
Mg#	0.40	0.68	0.35	0.68	0.56	0.68	0.58	0.68
TiO_2	1.64	0.39	1.74	0.24	1.00	0.53	0.96	0.63
K_2O	0.79	0.28	0.79	0.20	0.41	0.27	0.41	0.31
Sr	203	132	192	110	190	165	195	176
Y	33	7.7	44	6.1	22	12	22	15
Zr	117	27	153	20	74	39	67	44
Nb	6.3	1.4	7.6	1.0	3.5	1.8	3.3	2.1
Ba	188	61	220	49	114	70	102	73
La	11	2.7	13	1.8	6.7	3.6	5.6	3.7
Ce	25	6.1	31	4.6	16	8.6	14	9.3
Sm	4.0	0.95	5.1	0.70	2.8	1.5	2.2	1.5
Yb	3.1	0.76	4.1	0.60	2.1	1.1	1.9	1.2
Hf	3.1	0.74	4.1	0.58	2.1	1.1	1.9	1.3
Th	1.8	0.42	2.4	0.32	1.2	0.64	0.91	0.60
U	0.66	0.16	0.82	0.11	0.39	0.21	0.35	0.23

Table S1. Continued.

Sill	Tolstomysovskii							
Sample	887		888		891		3A	
	Meas.	Initial	Meas.	Initial*	Meas.	Initial	Meas.	Initial
Mg#	0.69	0.69	0.68	0.68	0.65	0.68	0.51	0.69
TiO_2	0.74	0.73	0.71	0.71	0.79	0.68	1.59	0.56
K_2O	0.28	0.28	0.27	0.27	0.31	0.28	0.46	0.24
Sr	168	167	177	177	187	179	227	193
Y	15	15	15	15	16	14	36	13
Zr	45	45	43	43	51	44	115	40
Nb	2.0	2.0	2.1	2.1	2.5	2.2	5.9	2.0
Ba	71	70	77	77	86	76	171	80
La	3.6	3.6	3.7	3.7	4.4	3.8	9.4	3.4
Ce	9.0	8.8	9.1	9.1	11	9.5	20	7.4
Sm	1.5	1.5	1.6	1.6	1.7	1.5	4.2	1.5
Yb	1.2	1.2	1.4	1.4	1.5	1.3	3.0	1.1
Hf	1.4	1.3	1.2	1.2	1.6	1.4	3.0	1.1
Th	0.56	0.55	0.64	0.64	0.73	0.63	1.1	0.39
U	0.24	0.24	0.23	0.23	0.30	0.26	0.51	0.18

Table S1. Continued.

Sill	China-Biryusinskii		Padunskii		Tulunskii		Usol'skii	
Sample	38-28		9/114y		T2		2843	
	Meas.	Initial	Meas.	Initial	Meas.	Initial	Meas.	Initial
Mg#	0.47	0.70	0.48	0.70	0.49	0.68	0.43	0.68
TiO_2	1.80	0.53	1.64	0.51	1.49	0.63	1.89	0.59
K_2O	0.57	0.26	0.53	0.25	0.43	0.23	0.45	0.20
Sr	240	193	229	184	252	199	212	150
Y	40	12	37	12	37	16	37	12
Zr	133	38	123	38	114	47	95	29
Nb	6.4	1.8	5.9	1.8	5.3	2.2	6.1	1.9
Ba	203	82	190	81	156	80	153	61
La	11	3.2	10	3.2	8.5	3.7	9.2	2.9
Ce	23	7.2	22	7.1	19	8.3	22	7.1
Sm	4.8	1.4	4.4	1.4	4.2	1.8	3.7	1.2
Yb	3.6	1.1	3.1	1.0	3.3	1.4	3.0	0.97
Hf	3.5	1.1	3.3	1.1	3.0	1.3	3.0	0.95
Th	1.3	0.37	1.2	0.37	1.1	0.44	1.3	0.39
U	0.56	0.17	0.48	0.15	0.49	0.21	0.54	0.17

Table S1. Continued.

Sill	Usol'skii							
Sample	2845		2847		2848		2854	
	Meas.	Initial	Meas.	Initial	Meas.	Initial	Meas.	Initial
Mg#	0.46	0.70	0.43	0.70	0.50	0.68	0.49	0.68
TiO_2	1.90	0.55	2.18	0.50	1.83	0.77	1.76	0.72
K_2O	0.64	0.29	0.72	0.28	0.48	0.26	0.53	0.28
Sr	209	168	194	151	227	180	219	172
Y	39	11	41	9.5	32	9.5	31	13
Zr	99	28	116	26	86	26	88	36
Nb	7.2	2.1	8.1	1.8	7.1	2.9	8.8	3.6
Ba	192	78	195	68	137	70	147	74
La	11	3.2	10.7	2.6	8.8	3.8	9.4	3.9
Ce	25	7.6	26	6.4	21.2	9.2	23	95
Sm	4.0	1.2	4.6	1.1	3.5	1.5	3.6	1.5
Yb	3.2	0.95	3.4	0.82	2.6	1.1	2.6	1.1
Hf	2.8	0.84	3.5	0.83	2.5	1.1	2.7	1.2
Th	1.5	0.45	1.6	0.37	1.4	0.58	1.6	0.64
U	0.60	0.18	0.67	0.16	0.55	0.23	0.68	0.28

Note: * Initial melt of sample 888 is assumed to be the same as the measured composition.

Table S2. Mineral/melt distribution coefficients used to calculate initial melt compositions. Values are the means of several determinations[14]. Asterisks mark extrapolated values.

Element	Olivine/Melt	Plagioclase/Melt
Ti	0.015*	0.037
K	0.003*	0.9*
Sr	0.012	2.4
Y	0.029	0.012
Zr	0.015*	0.0002
Nb	0.004	0.024
Ba	0.001*	0.69
La	0.0001*	0.12
Ce	0.024	0.097
Pr	0.031	0.077
Sm	0.016	0.048
Yb	0.053	0.0098
Hf	0.02	0.08
Th	0.01*	0.064
U	0.01*	0.078